

Article

# Hybridization of Layered Iron Hydroxide Nanoclays and Conducting Polymer for Controlled Oxygen Scavenger

Hyoung-Jun Kim <sup>1</sup>, Tae-Hyun Kim <sup>2</sup>, Jin Kuen Park <sup>3,\*</sup> and Jae-Min Oh <sup>1,\*</sup>

<sup>1</sup> Department of Chemistry and Medical Chemistry, College of Science and Technology, Yonsei University, Wonju 26493, Korea; hjun.kim@yonsei.ac.kr

<sup>2</sup> Department of Physics, Chemistry and Pharmacy, University of Southern Denmark, 5230 Odense, Denmark; thkim@sdu.dk

<sup>3</sup> Department of Chemistry, Hankuk University of Foreign Studies, Yongin 17035, Korea

\* Correspondence: jinkpark@hufs.ac.kr (J.K.P.); jaemin.oh@yonsei.ac.kr (J.-M.O.)

Received: 30 August 2018; Accepted: 20 September 2018; Published: 27 September 2018



**Abstract:** We suggest green rust (GR), one of layered nanoclays, as a potential oxygen scavenger. In order to achieve controlled oxygen scavenging ability, GRs were prepared with either sulfate or conducting polymer. X-ray diffraction (XRD) patterns showed that both GRs had hydrotalcite phase with slight differences in crystallinity upon anion type. X-ray adsorption spectra (XAS) indicated that the local structure of both GRs were similar regardless of the type of anion. On the other hand, zeta-potential values of GRs were different from each other according to the type of anion; GR with sulfate showed positive charge and GR with conducting polymer had slight negative charge due to the homogeneous hybridization. Scanning electron microscopy (SEM) also suggested that the hybridization of conducting polymer and GR was fairly homogenous without the formation of phase segregation or serious aggregation. According to the oxygen-scavenging activity test, GR with conducting polymer showed a retarded oxygen-scavenging rate compared with GR with sulfate due to protection and controlled oxidation-reduction by hybridized polymer. The current results suggested that the hybridization of nanoclay with conducting polymer could be utilized in long-term oxygen scavenging applications with a controlled oxidation-reduction reaction.

**Keywords:** green rust; conducting polymer; oxygen scavenging; retarding oxidation; food packaging

## 1. Introduction

Various food products are sensitive to the external environment such as microbial attack [1] and deterioration by atmospheric oxygen [2]. These inevitably result in depreciation and a decrease in consumers' preference [3]. Antimicrobial packaging has been suggested by introducing nanoclays or antibacterial moiety in the film [1,4,5]. Meanwhile, many researchers have studied gas barrier packaging or oxygen-scavenging materials enclosed in packaging. Svagan et al. reported that polylactide film with 40 bilayer coating of montmorillonite/chitosan reduced oxygen permeability by about 90–95% at 20–50% relative humidity (RH) [6]. The preparation of carboxymethylated microfibrillated cellulose film was suggested to achieve low oxygen permeability at low RH by Aulin et al. [7]. Another oxidation prevention strategy is to introduce oxygen-scavenging materials such as iron-based powder (iron oxide, ferrous carbonate and metallic platinum) [8,9], ascorbic acid with metal catalyst [10], and an enzyme combination (glucose oxidase and catalase) into food packaging [8]. Those oxygen scavengers are usually applied in the form of a sachet or film coating for the freshness of oxygen-sensitive food [9,11,12].

However, there still remain several limitations in the aforementioned approaches. Although oxygen barrier film is effective to prevent O<sub>2</sub> access, only small damage in the film resulted in the failure of O<sub>2</sub> prevention. Oxygen scavengers like iron oxides requires relatively high humidity for their action [8,13]. Other scavengers like ascorbic acid or an enzyme combination are relatively expensive and not easy to deal with in a packaging process due to their environmental sensitivity (pH, salt condition, temperature and etc.) [8,10]. Therefore, we tried to prepare an alternative oxygen scavenger which has a low precursor price, controllable oxidation-reduction property, etc.

Green rust (GR) is a kind of layered nanomaterial consisting of Fe<sup>2+</sup>/Fe<sup>3+</sup> mixed hydroxide layers and interlayer anion (Cl<sup>-</sup>, CO<sub>3</sub><sup>2-</sup> and SO<sub>4</sub><sup>2-</sup>) along with water. The structure is an analogue of layered double hydroxide, which is often referred to as an anionic nanoclay. The chemical composition of GR is similar to that of iron oxide; however, (1) its layered structure provides a larger surface for oxidation-reduction at the Fe<sup>2+</sup>/Fe<sup>3+</sup> centers than iron oxide; and (2) the intrinsic water moiety along the hydroxide layer enabled a facilitated oxidation-reduction reaction. In fact, the Fe<sup>2+</sup> in GR is quickly oxidized to Fe<sup>3+</sup> in the presence of O<sub>2</sub> to produce the goethite (FeOOH) phase. Thus, GR has high potential to capture O<sub>2</sub> in food packaging as an oxygen-scavenging material. The only limitation of GR is its fast oxidation rate under the existence of O<sub>2</sub>, and thus GR itself can only be utilized as an O<sub>2</sub> scavenger for short-term utility.

In order to overcome this problem and to control the oxidation-reduction reaction of GR, we tried to hybridize GR with a conducting polymer, poly(3,4-ethylenedioxythiophene) (PEDOT):poly(4-styrenesulfonate) (PSS), which have high electrical conductivity, transparency and thermal stability [14,15]. As the reduction potential of the conducting polymer would be slightly higher than Fe<sup>2+</sup>, the polymer would retard the oxidation rate of GR. Furthermore, the electron donor-acceptor behavior between GR and the conducting polymer would control the oxidation rate of GR.

In this study, we prepared GR with general anion, SO<sub>4</sub><sup>2-</sup>, and conducting polymer (PEDOT:PSS), to compare the oxygen-scavenging property depending on the interlayer anion. In particular, GR with a SO<sub>4</sub><sup>2-</sup> interlayer anion (GR-SO<sub>4</sub>) was selected as reference sample of GR without a conducting polymer, as GR-SO<sub>4</sub> is the most widely studied green rust in terms of structure and synthetic method. Through X-ray diffraction (XRD) patterns and X-ray absorption spectra (XAS) of both GRs, we confirmed the crystal and local structure of GR. In order to investigate the homogeneity in polymer distribution with GR, we measured the zeta-potential and scanning electron microscopic (SEM) images. Finally, we evaluated the time-dependent oxygen scavenging property of both GRs using O<sub>2</sub> gas analyzer using ambient gas condition.

## 2. Materials and Methods

### 2.1. Materials

Reagent grade ferrous sulfate heptahydrate (FeSO<sub>4</sub>·7H<sub>2</sub>O), ferric sulfate hydrate (Fe<sub>2</sub>(SO<sub>4</sub>)<sub>3</sub>·9H<sub>2</sub>O), poly(3,4-ethylenedioxythiophene) (PEDOT) and poly(styrenesulfonate) (PSS) were purchased from Sigma-Aldrich Co. LLC (St. Louis, MO, USA). Sodium hydroxide pellets (NaOH) were obtained from Daejung Chemicals & Metals Co., Ltd. (Siheung, Korea). All the chemicals were used without further purification.

### 2.2. Preparation of Green Rust (GR)-SO<sub>4</sub> and GR-PEDOT:PSS (GR-PEDOT)

For the preparation of GR-SO<sub>4</sub>, mixed divalent and trivalent iron solution (0.15 M of FeSO<sub>4</sub>·7H<sub>2</sub>O and 0.05 M of Fe<sub>2</sub>(SO<sub>4</sub>)<sub>3</sub>·9H<sub>2</sub>O) was titrated with 0.3 M of NaOH solution until pH reached ~6.9. This slurry was aged at room temperature for 24 h under N<sub>2</sub> atmosphere. The conductive polymer-introduced GR (GR-PEDOT) was prepared under the same ferri/ferrous stoichiometry as GR-SO<sub>4</sub> with an additional 5 mL of PEDOT:PSS solution (2.8 wt %). The alkaline solution was dropwisely added to the solution until pH ~6.9. The obtained product was stirred at room temperature

for 24 h under N<sub>2</sub> atmosphere. After 24 h, the final products were collected by centrifugation and lyophilized without washing process. Decarbonated water was used during synthesis process.

### 2.3. Characterization of GR-SO<sub>4</sub> and GR-PEDOT

The crystal structure of GR-SO<sub>4</sub> and GR-PEDOT was evaluated with a powder X-ray diffractometer (XRD; Bruker AXS D2 Phaser with LYNXEYE™ detector; Bruker AXS GmbH, Karlsruhe, Germany). The XRD patterns were measured with scanning range from 3° to 70° as following condition (1 mm air-scattering slit, a 0.1 mm equatorial slit, and time step increments of 0.02° and 0.5 s per step). The crystallite size was calculated using Scherrer's equation ( $\tau = K\lambda/\beta\cos\theta$ ,  $\tau$ : crystallite size (Å),  $K$ : dimensionless shape factor (0.9),  $\lambda$ : X-ray wavelength (1.5406 Å),  $\beta$ : full-width at half-maximum,  $\theta$ : Bragg angle). The surface charge of GR-SO<sub>4</sub> and GR-PEDOT was investigated using an ELSZ-1000 (Otsuka, Kyoto, Japan). For zeta-potential measurement, each sample powder was dispersed in deionized water (1 mg/mL) and then the prepared suspension transferred to a quartz flow cell with platinum electrode. The particle morphology of GR-SO<sub>4</sub> and GR-PEDOT was evaluated by scanning electron microscopy (FE-SEM; FEG Quanta250, FEI, USA). In order to obtain SEM images of samples, both powder samples were attached on carbon tape, and then sample surface was coated through Pt/Pd sputtering for 60 s. The SEM images were obtained under a 30 kV electron beam acceleration voltage with 10 mm working distance. The X-ray absorption near edge structure (XANES) and extended X-ray absorption fine structure (EXAFS) spectra were obtained using X-ray absorption spectroscopy (XAS) in the 8C beam line at the Pohang Accelerator Laboratory (Pohang, Korea). To obtain XAS spectra, a powder sample was attached between kapton tapes, and then X-ray absorption was measured around Fe K-edge energy (7112 eV). The gained EXAFS spectra was analyzed with XAFSVIEW package in order to examine the local structure and coordination state around Fe.

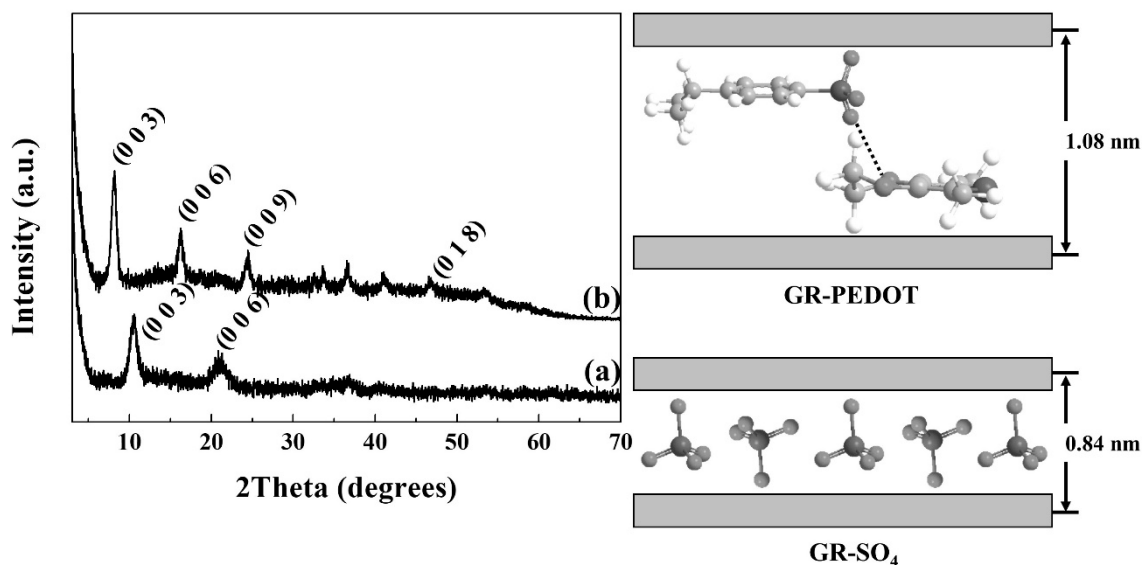
### 2.4. Oxygen-Scavenging Activity

In order to evaluate oxygen scavenging activity of GR-SO<sub>4</sub> and GR-PEDOT powder, both powders (0.6 g) were put in 60 mL volume airtight container which was previously filled with ambient air (~20 v% of O<sub>2</sub>). Then, the oxygen content of the internal container was measured using an O<sub>2</sub> Headspace gas analyzer (CheckMate 3, MOCON Inc., Minneapolis, MN, USA) in a time-dependent manner (10, 20, 30, 40, 50 and 60 min).

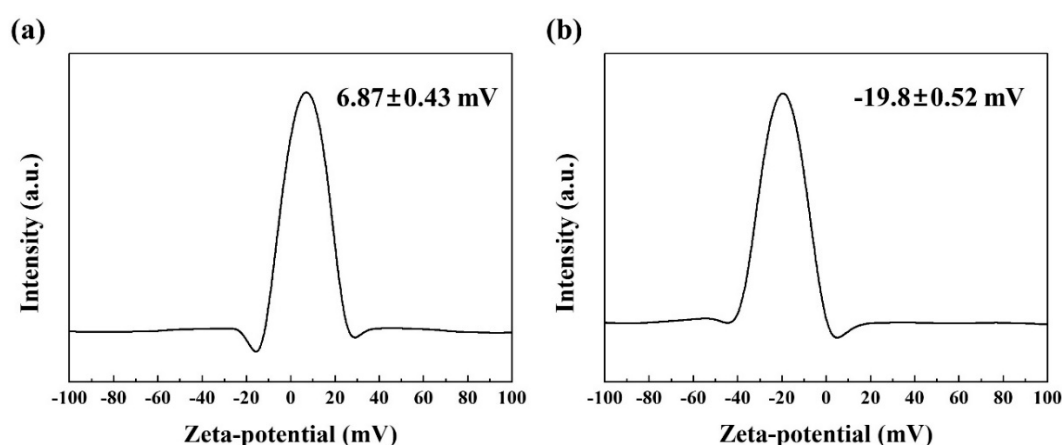
## 3. Results

Figure 1 represents powder X-ray diffraction patterns of GR with SO<sub>4</sub><sup>2-</sup> or with conducting polymer (PEDOT). The diffractogram of GR-SO<sub>4</sub>, sulfate intercalated green rust showed well developed (001) diffraction below 2 $\theta$  of 30° and several small lattice peaks above 2 $\theta$  of 30°. Similarly, the diffractogram of GR-PEDOT showed (001) peaks and lattice peaks, respectively. The d-spacings of both GRs calculated by (003) peak was 0.84 and 1.08 nm, respectively, showing correspondence with the molecular dimension of SO<sub>4</sub><sup>2-</sup> and PEDOT:PSS, respectively. It is notable that the GR-PEDOT showed a larger number of repeated (001) peaks with higher intensity than GR-SO<sub>4</sub>, which would be attributed to the different crystallinity of GR in the presence of the polymer. The crystallite sizes calculated by Scherrer's equation [16] utilizing (003) peaks were 7.36 and 10.5 nm for GR-SO<sub>4</sub> and GR-PEDOT, respectively. The (hkl) indexing followed the crystal phase of hydrotalcite (JCPDS NO.14-0191) as previously reported for green rust [17].

The surface charge of both GRs were evaluated by measuring its zeta potential in deionized water (Figure 2). The zeta potential of GR-SO<sub>4</sub> lay in the range of -10 mV to 30 mV, whereas that of GR-PEDOT was located between -40 mV and 0 mV. The full widths at half maximum of both samples were similarly narrow (~21 mV). The average zeta potential of GR-SO<sub>4</sub> and GR-PEDOT was  $6.87 \pm 0.44$  mV and  $-19.8 \pm 0.52$  mV, respectively, clearly showing respective positive and negative surface charge.



**Figure 1.** X-ray diffraction (XRD) patterns and corresponding schematic interlayer diagrams for (a) GR-SO<sub>4</sub> and (b) GR-PEDOT.



**Figure 2.** Zeta-potential graphs of (a) GR-SO<sub>4</sub> and (b) GR-PEDOT.

Scanning electron microscopy for both samples was carried out in order to observe particle size, morphology and homogeneity in phase (Figure 3). The image for GR-SO<sub>4</sub> showed relatively small particles with a size of 60 nm with some agglomeration. On the other hand, the particle of GR-PEDOT is larger and more plate-like than GR-SO<sub>4</sub>. The average particle size of GR-PEDOT was 140 nm and it also showed some agglomerations. In the SEM image of GR-PEDOT, we could not observe any serious aggregation of particles or lumps of polymers, indicating the PEDOT:PSS was well hybridized with the GR lattice without phase segregation. Energy-dispersive spectroscopy (EDS) mapping images showed the location of GR framework was overlapped with those of counter-anions. The locations of S, Fe, O (Fe, O from GR; S, O from SO<sub>4</sub><sup>2-</sup>) were well-overlapped in GR-SO<sub>4</sub>; the locations of C, S, Fe, O (Fe, O from GR; C, S, O from PEDOT:PSS) were also well-overlapped in GR-PEDOT (Figures S1 and S2). The photographic images of both GRs displayed in Figure 3 showed fine powdery state with greenish brown or black color, indicating the existence of Fe<sup>2+</sup>/Fe<sup>3+</sup> (for both samples) and PEDOT:PSS (in GR-PEDOT) in the powders.

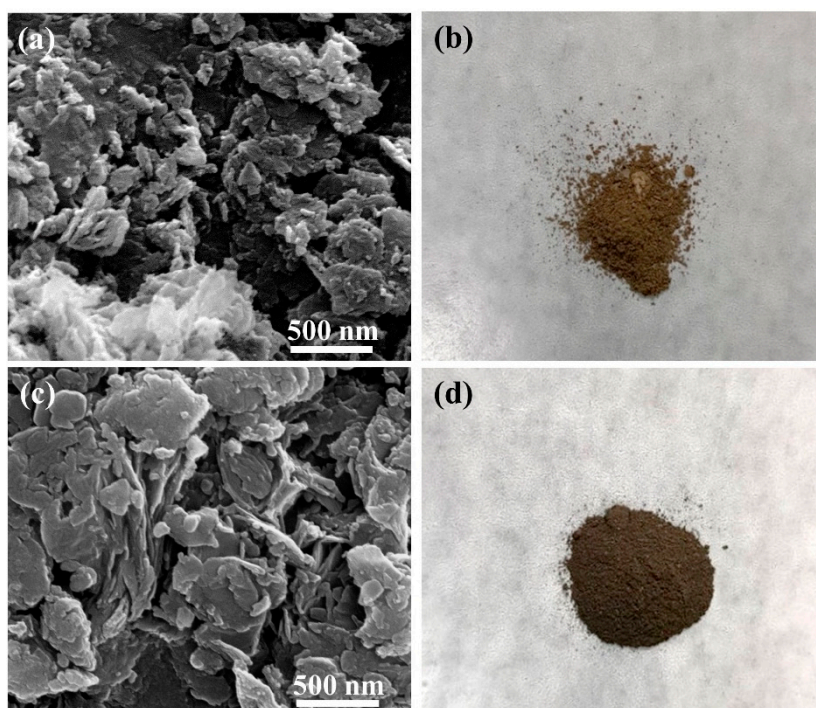


**Figure 3.** Scanning electron microscopic images and photograph for (a,b) GR-SO<sub>4</sub> and (c,d) GR-PEDOT.

Figure 4A showed XANES for GR-SO<sub>4</sub> and GR-PEDOT. Both spectra were similar in terms of peak shape and intensity. In particular, the pre-edge at 7114.04 eV and main edge at 7128.27 eV were commonly observed for both samples. The EXAFS in R-space was shown in Figure 4B. There could be observed a strong first shell peak at 1.4 Å (non-phase-shift corrected) and a relatively small second shell peak at 2.6 Å (non-phase-shift corrected), attributed to Fe–O and Fe–Fe bonds, respectively. The peak positions and shapes corresponded well to the EXAFS spectra of previously reported green rust [18,19].

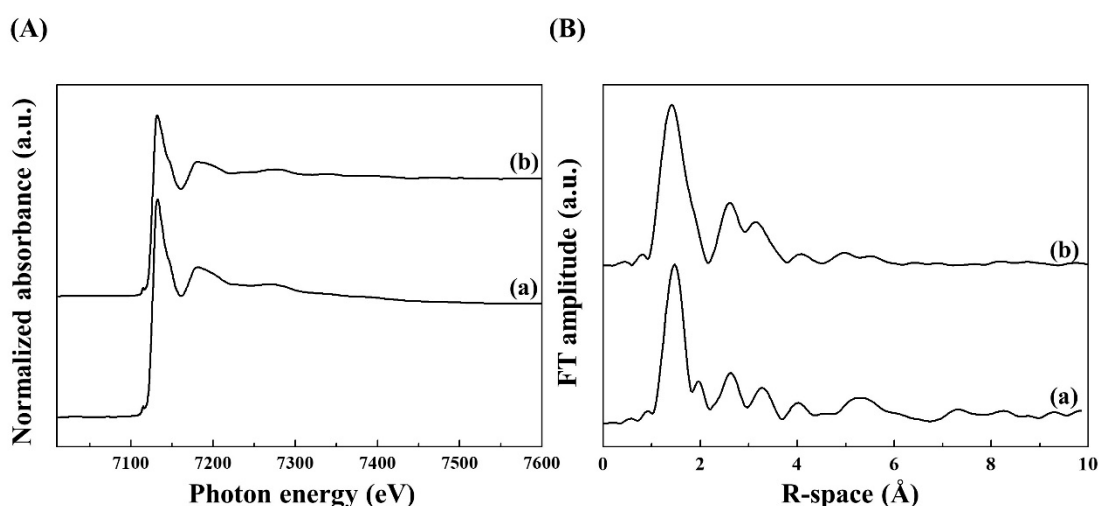


**Figure 4.** Fe K-edge (A) X-ray absorption near edge structure (XANES) spectra and (B) fourier-transformed X-ray absorption fine structure (EXAFS) spectra for (a) GR-SO<sub>4</sub> and (b) GR-PEDOT.

The oxygen-scavenging effect of GRs depending on different interlayer anions were evaluated in time-course (Figure 5). The test was carried out under ambient composition of air where ~20% of oxygen existed. At the early stage until 30 min, both GR-SO<sub>4</sub> and GR-PEDOT slowly removed O<sub>2</sub> showing O<sub>2</sub> partial pressure reduction by 97%. From the 30-min time point, both GRs showed different behavior; the partial pressure of O<sub>2</sub> abruptly decreased to 66% for GR-SO<sub>4</sub>. On the other

hand, the partial pressure of O<sub>2</sub> in the GR-PEDOT-containing vessel continuously decreased following a logarithm function. The fitted curve for O<sub>2</sub> partial pressure in the GR-PEDOT vessel is as follows;  $P = 99.4 - 0.725\ln(t - 6.93)$  (P: partial pressure of O<sub>2</sub>, t: time in min).

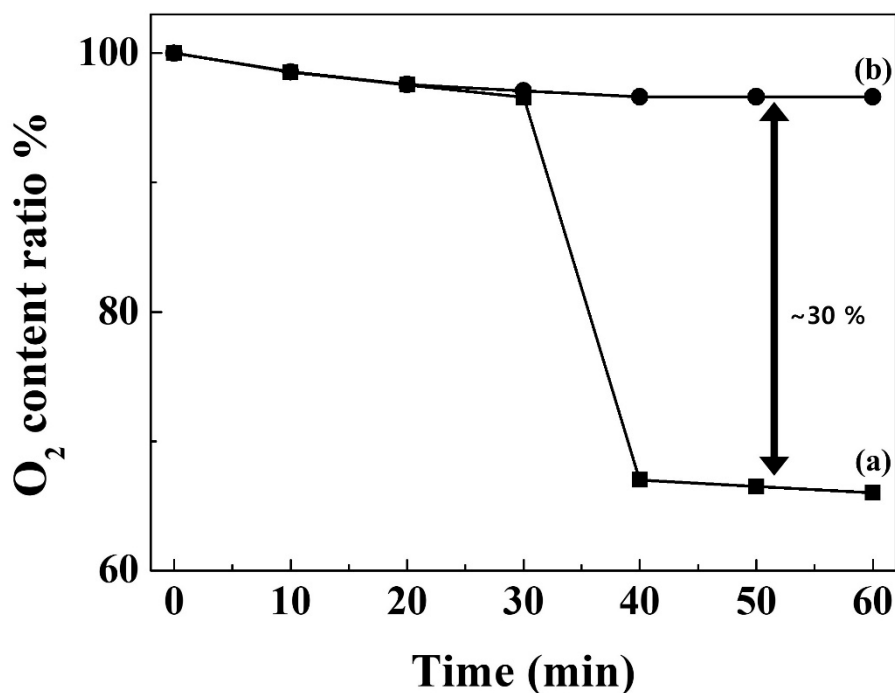
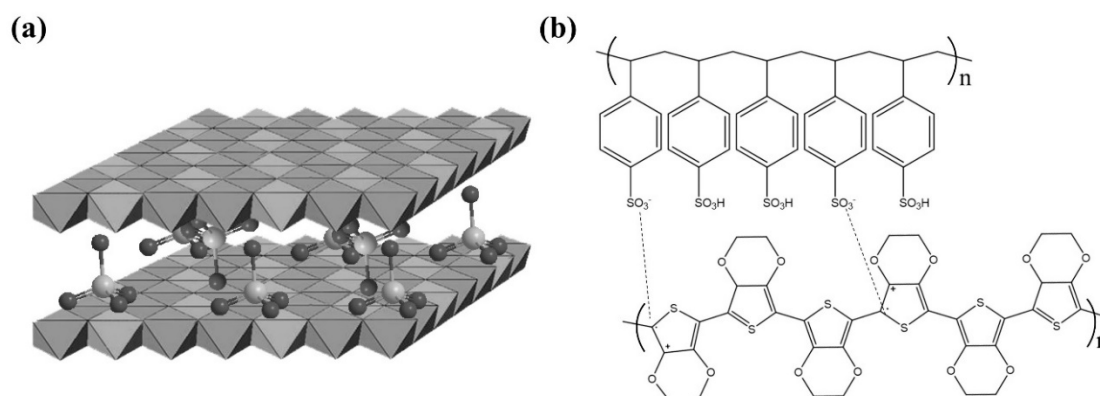


Figure 5. Remaining O<sub>2</sub> gas content ratio in airtight container for (a) GR-SO<sub>4</sub> and (b) GR-PEDOT.

#### 4. Discussion

This research aims to prepare green rusts (GRs) with different interlayer anions and to evaluate their structure as well as O<sub>2</sub> scavenging property. As shown in Scheme 1, the GR is composed of 2-dimensional layer and interlayer anions. The layers are composed of interconnected Fe(OH)<sub>6</sub> (either ferrous Fe<sup>2+</sup> or ferric Fe<sup>3+</sup>) octahedrons in an edge-sharing manner. GRs are usually prepared with an interlayer ion of sulfate [20] as shown in Scheme 1a, while other small inorganic acids like carbonate and chloride are possible in the interlayer space [21,22]. Incorporation of organic moiety or polymers are rare in GR systems; however, recently, we reported that a combination of PSS and polypyrrole could be accommodated in a GR lattice increasing the crystallinity of the host GR [23]. In the current study, we tried to intercalate a combination of conducting polymer (PEDOT:PSS) in order to exploit both the crystallinity increase and electron donation-acceptance property of conducting polymer.



Scheme 1. (a) Schematic structures of GR-SO<sub>4</sub> and (b) chemical structure of PEDOT:PSS.

As evidenced by X-ray diffractogram (Figure 1), both GRs were successfully prepared with either  $\text{SO}_4^{2-}$  or PEDOT:PSS interlayer anions. The slightly higher peak intensity and larger crystallite size for GR-PEDOT than GR- $\text{SO}_4$  were attributed to the crystal growth role of the polymer as reported previously [23]. The d-spacing of GR- $\text{SO}_4$  matched other literature well [23], while the d-spacing value of GR-PEDOT, a newly synthesized phase, corresponded to the molecular dimension of PEDOT:PSS. We hypothesized that the benzene moiety of PSS aligned parallel to the GR layer, while the anionic center of sulfonate groups head to the GR layer for charge compensating (Figure 1). As PSS acts as a dopant for PEDOT (Scheme 1b), the PSS and PEDOT moiety would be overlapped in the interlayer space of GR. Taking into account the molecular dimension of PSS and PEDOT, the current d-spacing of 1.08 nm (0.60 nm for gallery height +0.48 nm for GR's layer thickness) suggested that the GR layers were tightly holding the PEDOT:PSS moiety so that the electron transfer between PEDOT and GR layer could be feasible.

The positive zeta potential of GR- $\text{SO}_4$  (+6.87 mV) was attributed to the co-existence of  $\text{Fe}^{2+}$  and  $\text{Fe}^{3+}$  in the layer. The layer structure of GR could be understood from the brucite ( $\text{Mg}(\text{OH})_2$ ) layer. The substitution of  $\text{Fe}^{3+}$  for  $\text{Fe}^{2+}$  in a brucite-like layer, ferrous hydroxide ( $\text{Fe}(\text{II})(\text{OH})_2$ ), generated an excessive plus charge [24] resulting in positive zeta potential. It was noteworthy that GR-PEDOT had a negative charge surface about  $-19.8$  mV. According to the previous research of other groups, the surface charge of PEDOT:PSS was negative (around  $-80$ ~ $-89$  mv) at various PSS/PEDOT ratios due to coverage by the negatively charged PSS-rich layer [25,26]. As the surface of GR-PEDOT would be homogeneously covered with PEDOT:PSS, as the polymer does in the interlayer space, the zeta potential inevitably shifted to the negative region. We excluded the possibility that the PEDOT:PSS was simply mixed with GR particles. If that case occurred, the zeta potential of GR-PEDOT would be located in a more negative region (lower than  $-19.8$  mV) or two peaks, one for PEDOT:PSS and the other for GR, would be observed. The slight negative charge of GR-PEDOT compared with PEDOT:PSS indicated homogeneous hybridization between GR and PEDOT:PSS, hopefully through intercalation and surface coating. The SEM and EDS mapping images also convinced us that homogenous hybridization between PEDOT:PSS and GR was successful in GR-PEDOT (Figure 3 and Figure S2). We could clearly observe the grain of particles in SEM images of both GR- $\text{SO}_4$  and GR-PEDOT. Simple mixing between polymer and GR would result in two different morphologies in the microscopic image.

The photographs for powder revealed that both  $\text{Fe}^{2+}$  and  $\text{Fe}^{3+}$  co-exist in the synthesized GR samples (Figure 3). As the oxidation of  $\text{Fe}^{2+}$  to  $\text{Fe}^{3+}$  is spontaneous in terms of thermodynamics, goethite ( $\text{Fe}(\text{III})\text{OOH}$ ) impurity was often obtained during GR synthesis. The greenish color for both samples indicated that oxidation of  $\text{Fe}^{2+}$  was efficiently prohibited and the GR phase was obtained well. This result corresponded well to the XRD pattern (Figure 1) with only GR (hydrotalcite) peaks observed.

From XAS spectroscopy, we could confirm that the local structure of GR was not significantly affected by the type of intercalated molecules. The XANES spectra (Figure 4a) of both GRs showed same main edge ( $1s \rightarrow 4p$  transition) absorption [27], and thus the average oxidation state of Fe was almost similar to each other. There existed a pre-edge for both GRs, implying the potential Jahn–Teller distortion around Fe. Those kinds of pre-edge could be interpreted as symmetry that allowed  $1s \rightarrow 3d$  electron transition [18]. Although the  $\text{Fe}(\text{OH})_6$  in GR is considered to have octahedral geometry, the real symmetry is rather assigned to  $D_{3d}$  due to the packing of octahedrons [28]. In terms of the edge positions (pre-edge and main edge) as well as the shape of the white line, both GRs would have same local symmetry around Fe. The R-space EXAFS patterns were also similar for both GR- $\text{SO}_4$  and GR-PEDOT. This result indicated that the inter-atomic distances of both Fe–O and Fe–Fe were not affected by different interlayer molecules. It is, therefore, concluded that both GRs had the same structure of layer framework and different interlayer and/or surface chemistry.

The difference in interlayer anions is thought to influence the oxidation of  $\text{Fe}^{2+}$  in GR. The partial  $\text{O}_2$  pressure gradually decreased for both GR- $\text{SO}_4$  and GR-PEDOT until 30 min. After then, the pattern became different; GR-PEDOT kept gradual decreasing while GR- $\text{SO}_4$  decreased  $\text{O}_2$  partial pressure abruptly. At time point 60 min, the difference in  $\text{O}_2$  partial pressure between GR- $\text{SO}_4$  and

the GR-PEDOT treated group was ~30%. This result suggested that the oxidation of GR was retarded in the presence of the conducting polymer, PEDOT:PSS. Applying a time vs. O<sub>2</sub> pressure equation,  $p = 99.4 - 0.725\ln(t - 6.93)$  ( $p$ : partial pressure of O<sub>2</sub>,  $t$ : time in min), we could extrapolate that O<sub>2</sub> scavenging would continuously occur by GR-PEDOT for a prolonged time.

In general, the oxidation process of Fe<sup>2+</sup> (−0.506 V vs. saturated calomel electrode (SCE)) is thermodynamically favored combined with the reduction of oxygen (0.57 V vs. SCE) so that the green rust could be easily transformed to goethite (Fe(III)OOH) under ambient air as we reported in the previous literature [22]. However, the oxidation potential of PEDOT:PSS is relatively higher than that of Fe<sup>2+</sup> [29,30], and thus the oxidation of PEDOT by O<sub>2</sub> is less feasible than oxidation of Fe<sup>2+</sup>. The action of PEDOT on the GR surface could be (i) protecting GR from oxidation, and (ii) retarding oxidation by atmospheric O<sub>2</sub> through adjusted reduction potential. Therefore, it could be suggested that Figure 5a showed the oxygen-scavenging profile by the transformation of green rust to goethite without PEDOT:PSS but PEDOT:PSS could retard the oxidation as shown in Figure 5b.

## 5. Conclusions

In this study, we synthesized the GRs with an interlayer anion SO<sub>4</sub><sup>2−</sup> or PEDOT:PSS for comparing the oxygen-scavenging property depending on the interlayer anion of GRs. According to the XRD patterns of both GRs, we confirmed that both GRs have a hydrotalcite-like crystal structure and PEDOT:PSS was tightly bound in the interlayer of GR for GR-PEDOT. The Fe<sup>2+</sup>/Fe<sup>3+</sup> co-existing in GR-SO<sub>4</sub> have a positive surface charge, while PEDOT:PSS incorporated GR showed shifted surface charge to the negative region, attributed to homogeneous hybridization between GR and negative PEDOT:PSS. The SEM images of both GRs indicated that the GR-PEDOT had larger particle size compared with GR-SO<sub>4</sub> and that homogeneous hybridization between GR and the conducting polymer occurred without serious aggregation nor phase segregation. Through XAS spectroscopy, we verified the local structures of both GRs were almost same regardless of anion type. The oxygen-scavenging property of both GRs revealed that GR-PEDOT had retarded oxidation compared with GR-SO<sub>4</sub>, attributed to the action of PEDOT: protection as well as adjustment in reduction potential. This result suggested that the GR-PEDOT can be used for long-term oxygen scavenging with a controlled oxidation-reduction property. In order to realize a practical GR oxygen scavenger for food packaging, further studies on oxidation-reduction optimization depending on stoichiometry and surface properties will be carried out in the near future.

**Supplementary Materials:** The following are available online at <http://www.mdpi.com/2076-3417/8/10/1742/s1>, Figure S1: Scanning electron microscopic images and energy-dispersive spectroscopy mapping images of GR-SO<sub>4</sub>, Figure S2: Scanning electron microscopic images and energy-dispersive spectroscopy mapping images of GR-PEDOT.

**Author Contributions:** Performed the preparation: H.-J.K.; characterization of GRs: H.-J.K.; carried out oxygen-scavenging test of GRs: T.-H.K.; designed the concept of the study and drafted the manuscript: J.K.P.; designed the material preparation and experiment, and also drafted the manuscript: J.-M.O.

**Funding:** This work was supported by the Radiation Technology R&D program through the National Research Foundation of Korea funded by the Ministry of Science and ICT (NRF-2017M2A2A6A05093711), and by the National Research Foundation of Korea (NRF) grant funded by the Korean government (MSIT) (No. 2017R1A2B4006352).

**Conflicts of Interest:** The authors declare no conflict of interest.

## References

1. Makaremi, M.; Pasbakhsh, P.; Cavallaro, G.; Lazzara, G.; Aw, Y.K.; Lee, S.M.; Milioto, S. Effect of morphology and size of halloysite nanotubes on functional pectin bionanocomposites for food packaging applications. *ACS Appl. Mater. Interfaces* **2017**, *9*, 17476–17488. [[CrossRef](#)] [[PubMed](#)]
2. Gibis, D.; Rieblinger, K. Oxygen scavenging films for food application. *Procedia Food Sci.* **2011**, *1*, 229–234. [[CrossRef](#)]
3. Robertson, G.L. *Food Packaging: Principles and Practice*, 2nd ed.; Taylor & Francis: New York, NY, USA, 2005.

4. Biddeci, G.; Cavallaro, G.; Di Blasi, F.; Lazzara, G.; Massaro, M.; Milioto, S.; Parisi, F.; Riela, S.; Spinelli, G. Halloysite nanotubes loaded with peppermint essential oil as filler for functional biopolymer film. *Carbohydr. Polym.* **2016**, *152*, 548–557. [[CrossRef](#)] [[PubMed](#)]
5. Lisuzzo, L.; Cavallaro, G.; Lazzara, G.; Milioto, S.; Parisi, F.; Stetsyshyn, Y. Stability of halloysite, imogolite, and boron nitride nanotubes in solvent media. *Appl. Sci.* **2018**, *8*, 1068. [[CrossRef](#)]
6. Svagan, A.J.; Åkesson, A.; Cárdenas, M.; Bulut, S.; Knudsen, J.C.; Risbo, J.; Plackett, D. Transparent films based on pla and montmorillonite with tunable oxygen barrier properties. *Biomacromolecules* **2012**, *13*, 397–405. [[CrossRef](#)] [[PubMed](#)]
7. Aulin, C.; Gällstedt, M.; Lindström, T. Oxygen and oil barrier properties of microfibrillated cellulose films and coatings. *Cellulose* **2010**, *17*, 559–574. [[CrossRef](#)]
8. Cruz, R.S.; Camilloto, G.P.; dos Santos Pires, A.C. Oxygen scavengers: An approach on food preservation. In *Structure and Function of Food Engineering*; InTech: London, UK, 2012.
9. Miltz, J.; Perry, M. Evaluation of the performance of iron-based oxygen scavengers, with comments on their optimal applications. *Packag. Technol. Sci.* **2005**, *18*, 21–27. [[CrossRef](#)]
10. Buettner, G.R. In the absence of catalytic metals ascorbate does not autoxidize at pH 7: Ascorbate as a test for catalytic metals. *J. Biochem. Biophys. Methods* **1988**, *16*, 27–40. [[CrossRef](#)]
11. Cruz, R.S.; Soares, N.d.F.F.; Andrade, N.J.d. Efficiency of oxygen: Absorbing sachets in different relative humidities and temperatures. *Ciência e Agrotecnologia* **2007**, *31*, 1800–1804. [[CrossRef](#)]
12. Byun, Y.; Bae, H.J.; Whiteside, S. Active warm-water fish gelatin film containing oxygen scavenging system. *Food Hydrocoll.* **2012**, *27*, 250–255. [[CrossRef](#)]
13. Vermeiren, L.; Devlieghere, F.; van Beest, M.; de Kruijf, N.; Debevere, J. Developments in the active packaging of foods. *Trends Food Sci. Technol.* **1999**, *10*, 77–86. [[CrossRef](#)]
14. Du, Y.; Shen, S.Z.; Cai, K.; Casey, P.S. Research progress on polymer–inorganic thermoelectric nanocomposite materials. *Prog. Polym. Sci.* **2012**, *37*, 820–841. [[CrossRef](#)]
15. Zhang, W.; Zhao, B.; He, Z.; Zhao, X.; Wang, H.; Yang, S.; Wu, H.; Cao, Y. High-efficiency ito-free polymer solar cells using highly conductive pedot:Pss/surfactant bilayer transparent anodes. *Energy Environ. Sci.* **2013**, *6*, 1956–1964. [[CrossRef](#)]
16. Cullity, B.D.; Stock, S.R. *Elements of X-ray Diffraction*; Pearson Education: Upper Saddle River, NJ, USA, 2014.
17. Génin, J.-M.R.; Aïssa, R.; Géhin, A.; Abdelmoula, M.; Benali, O.; Ernstsens, V.; Ona-Nguema, G.; Upadhyay, C.; Ruby, C. Fougerite and feii–iii hydroxycarbonate green rust; ordering, deprotonation and/or cation substitution; structure of hydrotalcite-like compounds and mythic ferrosic hydroxide fe(oh)(2+x). *Solid State Sci.* **2005**, *7*, 545–572. [[CrossRef](#)]
18. Suzuki, S.; Shinoda, K.; Sato, M.; Fujimoto, S.; Yamashita, M.; Konishi, H.; Doi, T.; Kamimura, T.; Hashimoto, T.; Inoue, K. Characterization of reaction of green rust with foreign ions using x-ray absorption fine structure. *Zairyo-to-Kankyo* **2008**, *57*, 353–357. [[CrossRef](#)]
19. Pantke, C.; Obst, M.; Benzerara, K.; Morin, G.; Ona-Nguema, G.; Dippon, U.; Kappler, A. Green rust formation during fe(ii) oxidation by the nitrate-reducing acidovorax sp. Strain bofen1. *Environ. Sci. Technol.* **2012**, *46*, 1439–1446. [[CrossRef](#)] [[PubMed](#)]
20. Simon, L.; François, M.; Refait, P.; Renaudin, G.; Lelaurain, M.; Génin, J.-M.R. Structure of the fe(ii-iii) layered double hydroxysulphate green rust two from rietveld analysis. *Solid State Sci.* **2003**, *5*, 327–334. [[CrossRef](#)]
21. Génin, J.-M.R.; Bourrié, G.; Trolard, F.; Abdelmoula, M.; Jaffrezic, A.; Refait, P.; Maitre, V.; Humbert, B.; Herbillon, A. Thermodynamic equilibria in aqueous suspensions of synthetic and natural fe(ii)–fe(iii) green rusts: Occurrences of the mineral in hydromorphic soils. *Environ. Sci. Technol.* **1998**, *32*, 1058–1068. [[CrossRef](#)]
22. Nagata, F.; Inoue, K.; Shinoda, K.; Suzuki, S. Characterization of formation and oxidation of green rust (Cl–) suspension. *ISIJ Int.* **2009**, *49*, 1730–1735. [[CrossRef](#)]
23. Kim, M.-S.; Kim, T.-H.; Seo, Y.S.; Oh, J.-M.; Park, J.K. A novel synthesis of an Fe<sup>3+</sup>/Fe<sup>2+</sup> layered double hydroxide ('green rust') via controlled electron transfer with a conducting polymer. *Dalton Trans.* **2017**, *46*, 7656–7659. [[CrossRef](#)] [[PubMed](#)]
24. Guilbaud, R.; White, M.L.; Poulton, S.W. Surface charge and growth of sulphate and carbonate green rust in aqueous media. *Geochim. Cosmochim. Acta* **2013**, *108*, 141–153. [[CrossRef](#)]
25. Horii, T.; Hikawa, H.; Katsunuma, M.; Okuzaki, H. Synthesis of highly conductive pedot:Pss and correlation with hierarchical structure. *Polymer* **2018**, *140*, 33–38. [[CrossRef](#)]

26. Horii, T.; Hikawa, H.; Mochizuki, Y.; Okuzaki, H. Synthesis and characterization of highly conductive pedot/pss colloidal gels. *Trans. Mater. Res. Soc. Jpn.* **2012**, *37*, 515–518. [[CrossRef](#)]
27. Sarangi, R. X-ray absorption near-edge spectroscopy in bioinorganic chemistry: Application to M–O<sub>2</sub> systems. *Coord. Chem. Rev.* **2013**, *257*, 459–472. [[CrossRef](#)] [[PubMed](#)]
28. Rives, V. *Layered Double Hydroxides: Present and Future*; Nova Publishers: New York, NY, USA, 2001.
29. Gualandi, I.; Marzocchi, M.; Scavetta, E.; Calienni, M.; Bonfiglio, A.; Fraboni, B. A simple all-pedot:Pss electrochemical transistor for ascorbic acid sensing. *J. Mater. Chem. B* **2015**, *3*, 6753–6762. [[CrossRef](#)]
30. Park, H.-S.; Ko, S.-J.; Park, J.-S.; Kim, J.Y.; Song, H.-K. Redox-active charge carriers of conducting polymers as a tuner of conductivity and its potential window. *Sci. Rep.* **2013**, *3*, 2454. [[CrossRef](#)] [[PubMed](#)]



© 2018 by the authors. Licensee MDPI, Basel, Switzerland. This article is an open access article distributed under the terms and conditions of the Creative Commons Attribution (CC BY) license (<http://creativecommons.org/licenses/by/4.0/>).